Investigation of the properties of alkali-activated slag mixes involving the use of nanoclay and nucleation seeds for 3D printing

Biranchi Panda[1,3], Shaoqin Ruan[2], Cise Unluer[2,4*], Ming Jen Tan[1]

[1] Singapore Centre for 3D Printing, School of Mechanical & Aerospace Engineering, Nanyang Technological University, 50 Nanyang Avenue, Singapore 639798

[2] School of Civil and Environmental Engineering, Nanyang Technological University, 50 Nanyang Avenue, Singapore 639798

[3] Department of Mechanical Engineering, Indian Institute of Technology Guwahati, Guwahati, India

[4] School of Engineering, University of Glasgow, G12 8LT, Glasgow, United Kingdom

* Corresponding author. E-mail address: Cise.Unluer@glasgow.ac.uk

Abstract:

This study investigated the properties of alkali activated slag (AAS) binders formulated for extrusion-based 3D printing. The fresh properties of AAS mixes were tailored through the use of nanoclay (NC) and nucleation seeds. The printability criteria employed were the ease of extrusion (extrudability) and the stability of the layered structure (buildability). Introduction of 0.4% NC in AAS mixes led to improved thixotropic properties due to the flocculation effect, which accounted for the extrudability and shape fidelity of the binder. Inclusion of 2% hydromagnesite seeds in this mix design provided additional nucleation sites for the increased precipitation of hydrate phases, resulting in denser microstructures. This enhanced the hydration reaction and improved the structural build-up rate necessary for large-scale 3D printing. The developed AAS mix containing 0.4% NC and 2% hydromagnesite seeds was used in the printing of an actual 3D structure to demonstrate its feasibility to be used in 3D printing applications.

Keywords: Alkali-activated slag; 3D printing; rheology; hydration; strength

1. Introduction

Extrusion-based additive manufacturing, also known as 3D printing, enables the mould-free fabrication of complex customized parts, which cannot be easily processed by other conventional manufacturing methods [1-4]. This technology has been successfully applied in aerospace, automotive and biomedical fields, while it is still being researched in the construction sector. The expected benefits of 3D concrete printing are higher productivity, shorter construction periods, higher geometrical freedom and more efficient use of natural resources [5]. The use of 3D printing can also present advantages in terms of reduced costs in the case of complex structures, in comparison to the conventional construction methods.

A pivotal approach in the success of 3D printing in construction is the use of Building Information Modelling (BIM). Since BIM already serves as a rich source of geometric information for existing structures, on site 3D concrete printing will eventually need scheduling and assembly sequence information to maintain safety and productivity [6, 7]. Previous studies [8] that shared this vision proposed a shift to a digital construction organization by combining existing technologies such as rapid digital mapping, BIM, digital collaboration, internet of things and design to construction. To further digitalise the construction industry, digital twin technology can be used to continuously monitor progress against the schedule laid out in the BIM model. Furthermore, approaches such as the digital twin technology can be combined with 3D concrete printing to reduce the volume of trial and error testing, reduce defects and shorten the time between the design and production processes [9].

While the use of cement-based materials in 3D printing presents several advantages, certain challenges need to be resolved for a successful printing process. To be used for printing applications, the rheology of cement-based mixes must meet certain requirements. Accordingly, during extrusion, the material must be fluid to prevent any blocking, bleeding or segregation. However, once they are printed, each layer must be able to harden quickly to support the superposed layers [10]. Another parameter to be considered is the time gap between printed layers. Long time gaps can provide an adequate mechanical strength for supporting the weight of the subsequently deposited layers, while short time gaps ensure optimized bonding strength.

Therefore, for successful printing, a narrow process window in terms of material yield stress exists, as shown in Fig. 1, where a schematic of extrusion-based additive manufacturing of cement-based mixes is demonstrated. Accordingly, the rheology of the developed mixes needs to be adjusted to achieve a minimum yield stress for smooth extrudability. After extrusion, the yield stress must evolve faster than the stress acting on the bottom layer to avoid strength-based failures. Alternatively, materials with a high yield stress can result in poor interlayer bonds, despite their ability to support additional layers.

Incorporation of reinforcement into the concrete matrix during the printing process is one of the most challenging issues needed to be dealt with to enable structural applications of 3D printing technology [11, 12]. In terms of materials, most of the printable mixtures contain ordinary Portland cement (PC) as the prime binder material due to its inherent thixotropic properties that originate from the combined effect of interparticle, gravitational and inertial forces [13-17]. However, as the production of PC accounts for 5-7% of the total anthropogenic CO_2 emissions, alternative cementitious materials are being investigated for their suitability to be used in 3D printing. Recent studies [18-21] have demonstrated the use of cementitious industrial by-products to reduce the carbon footprint of PC in 3D printing applications. As a part of these initiatives, the importance of proper rheology control for smooth extrusion and higher buildability properties was highlighted.

In line with these initiatives, this study aims to investigate the use of alkali-activated slag (AAS) mixes in 3D printing applications to contribute to the development of a sustainable built environment. To enable this, the prepared AAS formulations included nanoclay due to its thixotropic properties [23]. Furthermore, nucleation seeds (i.e. hydromagnesite) were also included to improve the rheological and mechanical properties of AAS [24, 25]. Accordingly, previous research [26] has shown that the use of seeds can provide additional nucleation sites for the increased precipitation of hydrate phases, thereby enhancing the rate and degree of the hydration reaction. To study the effect of these additives, nanoclay was first introduced into AAS mixtures for improved printability. An initial assessment of the fresh properties led to the determination of the mix with the highest yield stress and lowest viscosity. Once this mix was determined, different dosages (i.e. 1-2% by mass of slag) of hydromagnesite seed was introduced into the mix design. X-ray diffraction (XRD) and field emission scanning electron microscopy

(FESEM) were employed to analyse the formation of hydration products and investigate the microstructural development at the end of the curing process.

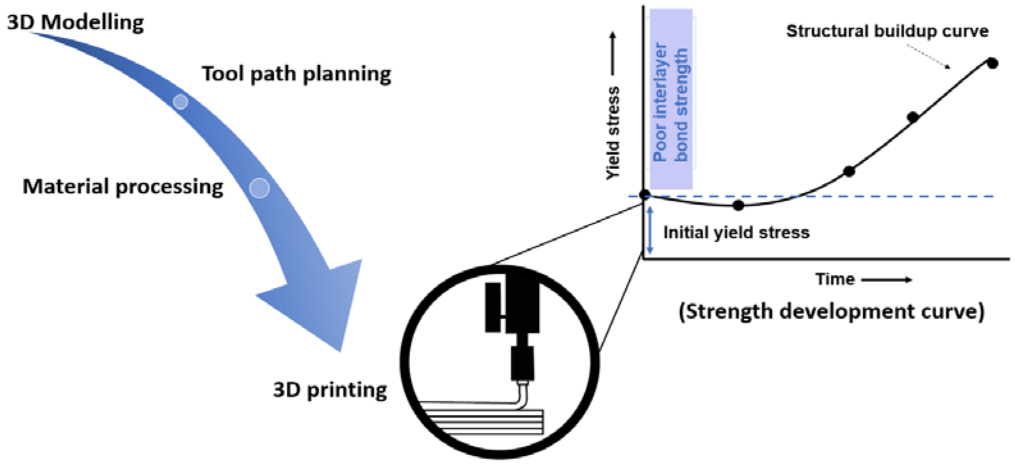

Fig. 1 Schematic of extrusion-based additive manufacturing of cement-based mixes

2. Materials and Methodology

2.1 Raw materials and sample preparation

The primary material utilized in this study was ground granulated blast-furnace slag (GGBS), provided by EnGro Corporation (Singapore). The chemical and physical properties of GGBS are shown in Table 1. The alkali activator was solid sodium metasilicate ($Na_2SiO_3 \cdot 5H_2O$), obtained from VWR (Singapore). Nanoclay (NC), a thermal treated, highly purified attapulgite clay supplied by Actigel (USA), was used to improve the thixotropy of the AAS binder. As can be seen from Fig. 2(a), NC particles agglomerated into clusters of different size composed of a pleated spherical morphology. Hydromagnesite ($4MgCO_3 \cdot Mg(OH)_2 \cdot 4H_2O$) seeds, obtained from Fisher Scientific (UK) with a specific surface area of 43.5 m^2/g, were used as nucleation seeds to stimulate the nucleation and growth of hydration products. The SEM image of hydromagnesite (Fig. 2(b)) demonstrated these seeds as spherical agglomerations with a diameter of ~1-7 µm, composed of

~0.5 µm diameter disks [24]. Fine aggregates with a maximum particle size of 1.18 mm was used in a saturated surface dry (SSD) condition to formulate the AAS mortars.

Table 1 Chemical composition and physical properties of GGBS.

	Chemical composition (%)							Physical properties	
	SiO_2	Al_2O_3	CaO	MgO	SO_3	TiO_2	LOI	Specific gravity (g/cm^3)	Blaine surface area (m^2/g)
GGBS	29.65	15.56	39.37	7.54	4.32	1.75	4.0	2.85	> 300

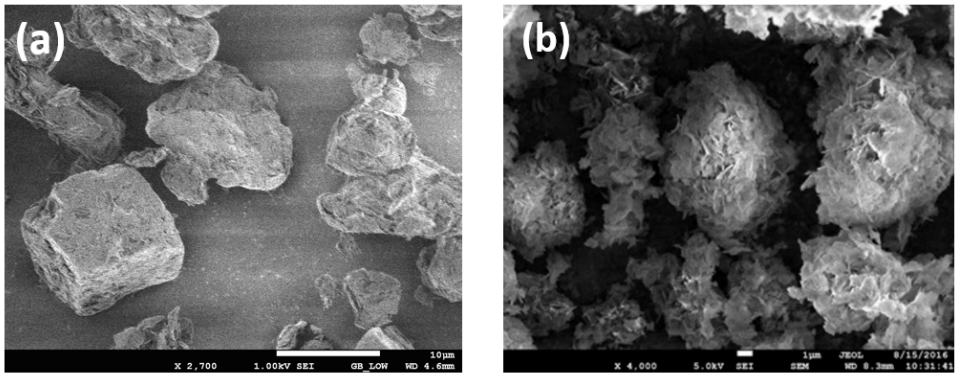

Fig. 2 SEM images of (a) nanoclay and (b) hydromagnesite seed [20]

The AAS used in this study was composed of only GGBS and 10% activator (i.e. by mass of slag) in line with the findings of a previous study [26]. Mixtures were prepared using water to binder (w/b) ratios of 0.35 and 0.40 for all pastes and mortars (i.e. at a sand/binder ratio of 0.83), respectively. AAS mortars without NC were prepared by adding water to the slag and sand mixture and mixed until a homogenous blend was obtained. For the preparation of mixes containing NC, NC was first blended into the predetermined amount of water for 3-4 minutes, after which it was added into the slag and sand mix and further mixed for another 2 minutes to ensure effective dispersion. For mixes involving the use of seeds, the seeds were first dispersed in half of the required total water and added into the mix, followed by the addition of NC, which was mixed with the remaining water.

2.2 Methodology

2.2.1 Static yield stress

A commercial rheometer (Anton-Paar MCR 102) was used to measure the static yield stress of the prepared AAS mortars. To initiate the study, freshly prepared AAS mortars were loaded in a measuring cup. Stress growth test was then performed by applying deformation at a constant shear rate of 0.1 s^{-1}. The shear stress progressively developed to a maximum value, followed by its decline to reach an equilibrium value. The static yield stress was defined as the peak shear stress value [27].

2.2.2 Thixotropy (shear thinning and viscosity recovery)

Thixotropy is an important property of printable materials, which can be characterized by a high viscosity at low stress and vice versa [39]. While there are various methods to quantify thixotropy, the "viscosity recovery" test was used to measure the thixotropy of AAS mixtures in this paper. Shear thinning property was measured by applying a constant shear rate of 300 s^{-1}, while viscosity recovery was measured by following a three-stage protocol, as previously described in [28]. The three stages and their respective shear rates and shearing timings were decided by mimicking the concrete printing process, where the state of the material starts from rest (i.e. at hopper) followed by high shear (i.e. extrusion) and finally ends at rest (i.e. on print bed). Fig. 3 shows the schematic of the protocol used for the evaluation of viscosity recovery. In addition to thixotropy, the structural build-up rate was also calculated from the evolution of static yield stress after 0, 5, 10 and 15 minutes of rest, which was used to assess the buildability property of the AAS mortars.

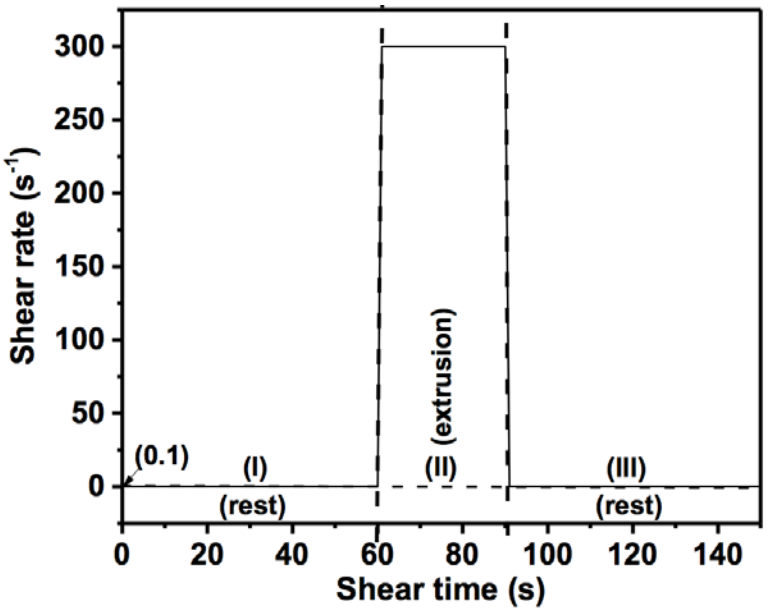

Fig. 3 Viscosity recovery protocol for measuring the thixotropy of AAS mortars

2.2.3 3D printing

The printability criteria employed in this study were: (i) ease of extrusion through a rectangular nozzle (i.e. extrudability) and (ii) stability of the layered printed filament (i.e. buildability). A 4-axis gantry printer [29] was used to test the extrudability of AAS mortars using a 30 (L) x 15 (W) mm nozzle. The printer was connected to a screw pump and the print speed was varied from 60 to 100 mm/sec at a constant flow rate to find the optimum speed for better shape stability of the filaments. This was followed by the printing of a hollow cylinder with the optimum combination of flow rate and speed to demonstrate the buildability of the AAS mortar.

2.2.4 Microstructural characterization (XRD and FESEM)

Samples extracted from AAS pastes were stored in acetone to stop hydration, followed by vacuum drying in preparation for XRD and FESEM analyses. XRD was recorded on a Philips PW 1800 spectrometer using Cu Kα radiation (40 kV, 30 mA), with a scanning rate of 0.04° 2θ/step from

10 to 70° 2θ. FESEM was carried out with a Zeiss Evo 50 microscope to investigate the morphologies of the hydration products. The vacuum dried samples were mounted onto aluminium stubs using double-sided adhesive carbon disks and coated with gold before FESEM analysis.

3. Results and Discussion

3.1 Effect of nanoclay on extrusion rheology

Printability is defined as the ability of a mixture to be extruded (i.e. extrudability) and maintain its structural integrity when built in layers (i.e. buildability) [10, 32]. In this respect, yield stress is an important rheological parameter that influences printability. Similarly, viscosity of a mixture is also related to its extrudability. Therefore, the yield stress and viscosity values obtained from a rotational rheometer were synergistically considered to analyse the printability of the prepared AAS mixes. Fig. 4 shows the effect of the inclusion of different amounts of NC on the static yield stress and apparent viscosity of AAS mortars. AAS mixes usually demonstrate low yield stress values due to the absorption of silicate anions (i.e. from the activator) on the slag surfaces, which results in strong double-layer repulsive forces between the slag particles, thereby causing particle separation and a low yield stress [31]. However, when compared to the control mix (0% NC), an increase in the NC content led to a higher static yield stress. Accordingly, the inclusion of a small amount of NC (0.4%) was sufficient to increase the yield stress by higher than three times when compared to the control mix. Therefore, the addition of NC enabled rapid flocculation, making it an ideal thixotropic material for 3D printing applications.

While the use of NC increased the yield stress of AAS mixes, the apparent viscosity remained relatively constant under different NC contents. This could be useful in providing a smooth extrusion and deposition of the prepared mix, maintaining the shape fidelity of the filaments. Such unique behaviour of NC is attributed to the flocculation phenomena that controls the rheology, depending on the applied shear forces at different stages of concrete printing [32]. Accordingly, NC particles carry a negative and positive charge on their opposite ends. They tend to associate with each other by electrical attraction when the material is at rest. NC also presents a higher initial

viscosity at rest, which then decreases under strong pre-shearing as the structure breaks down [33]. Amongst the mixes prepared, since the addition of 0.6% NC resulted in the maximum yield stress that was measurable by the rheometer, this was the highest amount of NC introduced into the prepared AAS mortars in this study. However, as it provided the highest yield stress within the extrudable limit (< 8 KPa), a NC dosage of 0.4% was selected as the optimum amount for subsequent analyses. Alternatively, the addition of 0.6% NC led to the extrusion of a discontinuous filament, which could negatively affect the interlayer bond strength due to the high yield stress of the mixture.

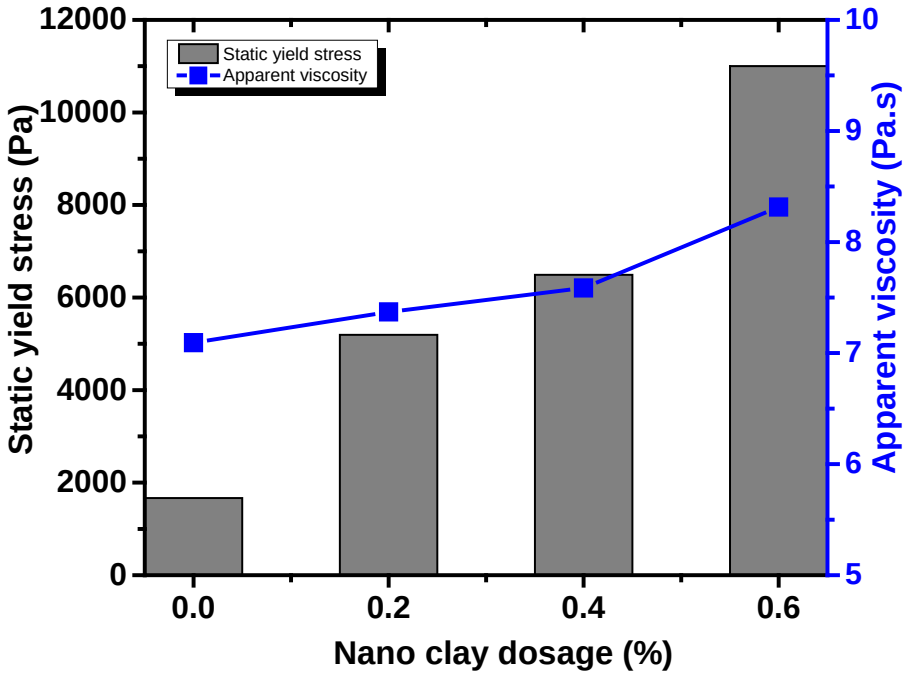

Fig. 4 Static yield stress and apparent viscosity as a function of NC dosage

Fig. 5 shows the flow curves over a range of shear rates (1−300 s^{-1}) for AAS motors with and without the addition of 0.4% NC. A shear-thinning behaviour was observed in both samples, which indicated increased viscosities with decreasing shear rates. When compared to the control mix, the NC modified mix resulted in higher viscosities at low shear rates, which could be helpful in maintaining the shape of the filament and support more layers. Alternatively, both mixtures demonstrated comparably low viscosities at high shear rates, which could enable a smooth

concrete flow without any discontinuity in the filament deposition. These results have demonstrated the role of NC in contributing to the development of more rigid AAS mixes via the flocculation of clay, resulting in mixes with high viscosities at low shear rates and vice versa.

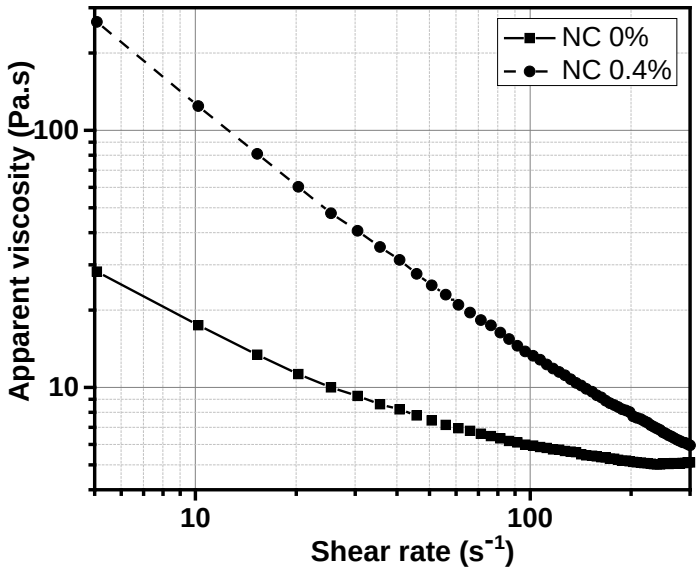

Fig. 5 Viscosity as a function of shear rate for the control (0% NC) and 0.4% NC modified AAS mortars

In order to be ideal for extrusion based printing purposes, a material should be highly thixotropic [10, 34]. In this respect, a low viscosity under a high shear force and the recovery of the viscosity to its original value after the removal of the shear force are preferable. Therefore, it is important to know how fast a deposited AAS mortar can recover its initial viscosity before the next layer is printed. Accordingly, Fig. 6 shows the viscosity recovery curves of AAS mortars including different amounts of NC. Although the initial viscosity (i.e. at stage I) of the control sample was higher, its recovery ability after strong shearing (i.e. at stage III) was much lower. This difference, shown by the blue arrow mark (Fig. 6), was an indication of the low recovery property of the control sample, which would negatively affect its shape retention after deposition as the viscosity after extrusion reduced due to poor recovery ability. On the other hand, mixes including NC revealed significantly better recovery properties, as shown by the red arrow mark (Fig. 6). The improved recoveries of these samples were attributed to the thixotropic property of NC. Amongst

the prepared samples, AAS including 0.4% NC was chosen for the assessment of its printability and structural build-up property due to its extrudable nature and 25% higher recovery ability than the control mix (0% NC).

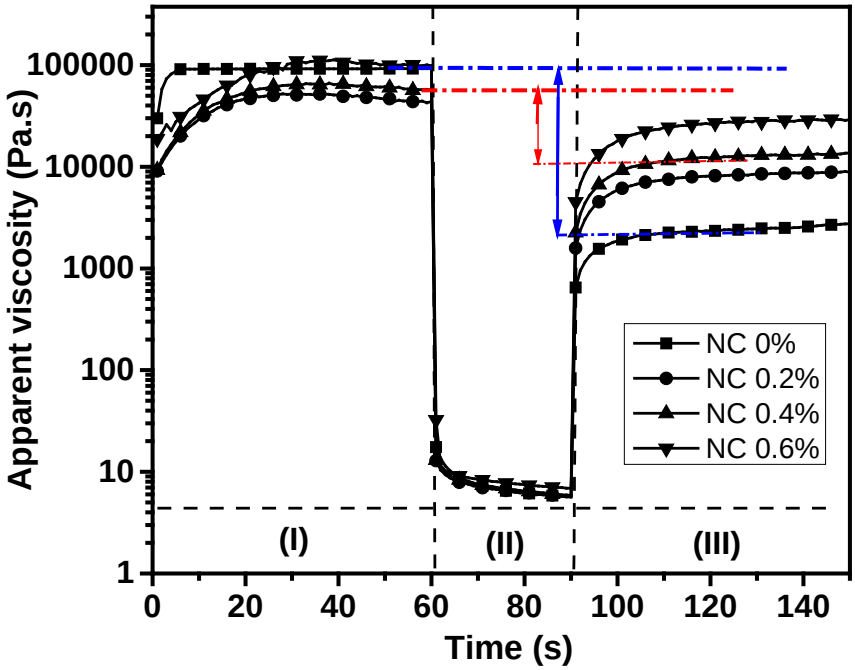

Fig. 6 Effect of the NC on the viscosity recovery of AAS mixtures

3.2 3D printing

3D printing of cementitious materials is a complex process, during which material properties, part design and process parameters interact with each other and define the characteristics of the final product. Process parameters like printing speed, nozzle shape and flow rate have a strong impact on the dimensional accuracy and mechanical properties of the final product [3, 29]. Fig. 7(a) shows the effect of printing speed (i.e. ranging between 60-100 mm/sec) on the dimensional accuracy of the filaments, while flow rate was kept constant. The printing process revealed that the printing speed and flow rate were dependant on each other. Accordingly, at each flow rate, there was an optimum speed that enabled the production of filaments with the same dimension as the nozzle

inlet. An increase or decrease in the speed beyond this optimum value would cause extra or insufficient material deposition, respectively. Out of the trials performed, setting the printing speed to 90 mm/s resulted in extrudates with a width (W) that was equivalent to the nozzle dimension (30 mm). Therefore, to demonstrate the possibility of using the developed AAS mortars in 3D printing applications, this speed was used in the printing of a cylinder with a diameter of 20 cm. Accordingly, the AAS mix containing 0.4% NC was printed up to 15 layers without the deformation of the bottom layer, as shown in Fig. 7(b). The deformation during printing can also be simulated by using optical techniques based on digital photogrammetry or terrestrial laser scanning, as discussed in previous studies [34].

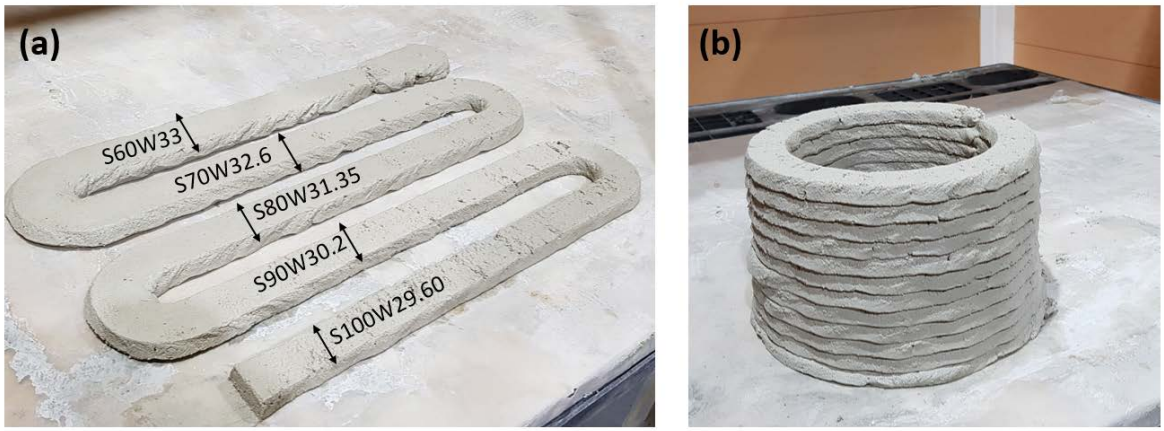

Fig. 7 3D printing of AAS mix containing 0.4% NC, showing the effect of: (a) printing speed on filament dimension and (b) buildability of several layers

3.3 Time-dependent rheological properties

The rheology of the material changes with time according to binder chemistry and presence of additives. The evolution of rheology with time is an important parameter for the printing process since fresh concrete is deposited in a layer-by-layer manner. This necessitates the material to possess fresh properties that can provide a 3D printed structure with structural stability [35]. Depending on the printing volume and speed, the material can be tailored to gain sufficient strength

before the printing of subsequent layers. The early strength of the material can be indirectly measured from its yield strength. Accordingly, Fig. 8 shows the yield stress values of the control AAS mix and the AAS mix containing 0.4% NC at different time intervals, obtained directly from the stress growth test. The inclusion of NC was found to increase the static yield stress of AAS mixes, revealing values that were three times higher than those of the control mix. This improvement in the yield stress was associated with the flocculation of NC particles, as discussed earlier in Section 3.1.

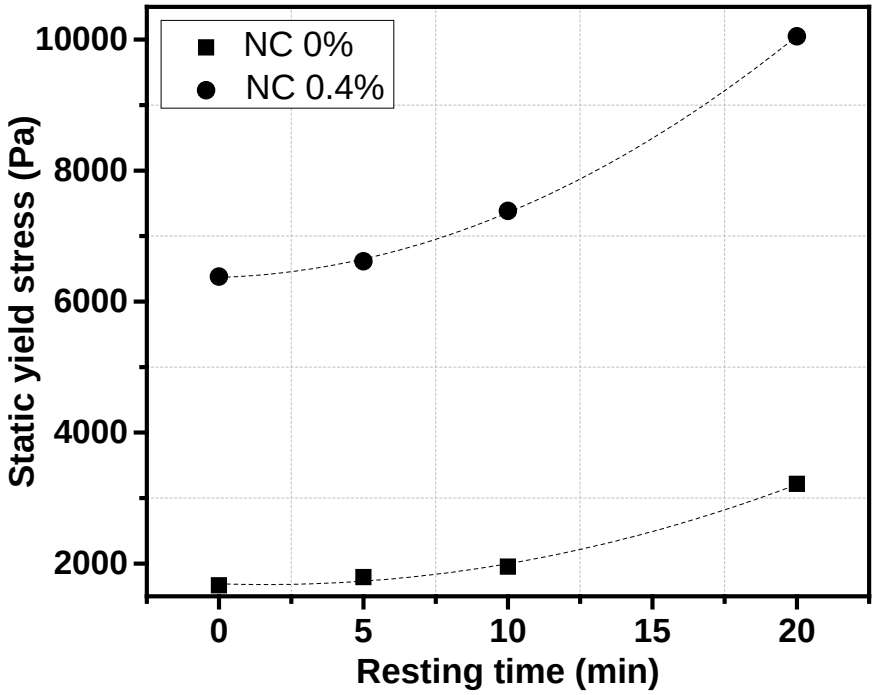

Fig. 8 Evolution of the static yield stress of AAS mortars with and without 0.4% NC

Alternatively, the rate of change of yield stress over time, also known as the structural build-up rate, was not significantly affected by the addition of clay. AAS mix containing 0.4% NC progressively gained yield stress, similar to the control sample. This observation was in line with the findings of previous studies [32, 33], where the addition of NC was reported to have an immediate impact on the yield stress, but have little or no influence on the rate of change of the yield stress over time. To overcome this issue, an accelerator can be added into AAS mixtures, which will enhance the build-up rate by accelerating the chemical (i.e. hydration) reaction.

Previous studies [24-26] have shown that nucleation seeds such as Ca- or Mg-based hydrate/carbonate phases can provide additional nucleation sites for the rapid and increased growth of hydration products. Therefore, different amounts of hydromagnesite ($4MgCO_3 \cdot Mg(OH)_2 \cdot 4H_2O$) seeds were introduced into the AAS mix containing 0.4% NC to investigate their effectiveness in improving the build-up rate and early age mechanical properties.

Fig. 9 shows the effect of 1% and 2% seed addition into the AAS mortar with and without the use of NC. Along with the findings of previous studies, where it was revealed that high seed contents were not effective due to dispersion issues [24, 25], only up to 2% seed addition was investigated in this study. Although the seed dosage had a little effect on the yield stress of both mixes, its influence on increasing the rate of change of yield stress over time, which can enhance the buildability of the printed structure without the need for any additional admixtures, should be evaluated before any final conclusions on the effectiveness of seeds could be made. Accordingly, Fig. 10 shows a successfully printed twisted column involving the use of the AAS mix containing 0.4% NC and 2% hydromagnesite seeds. As a part of this approach, a slender column was printed directly from the CAD model demonstrated in Fig. 10(a). This process was completed without any significant bottom layer deformation, as can be seen in Fig. 10(b). While this was an indication of the necessary stiffness of the AAS mix in resisting deformation imposed by top layers, its higher stiffness resulted in a rough surface texture, which could be improved for better printing results.

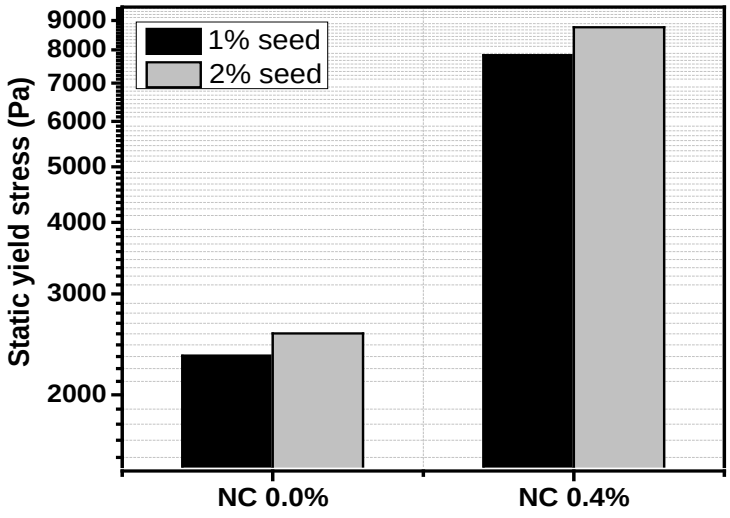

Fig. 9 Effect of nucleation seeds on the yield stress of AAS mixes containing 0.4% NC, obtained just after mixing

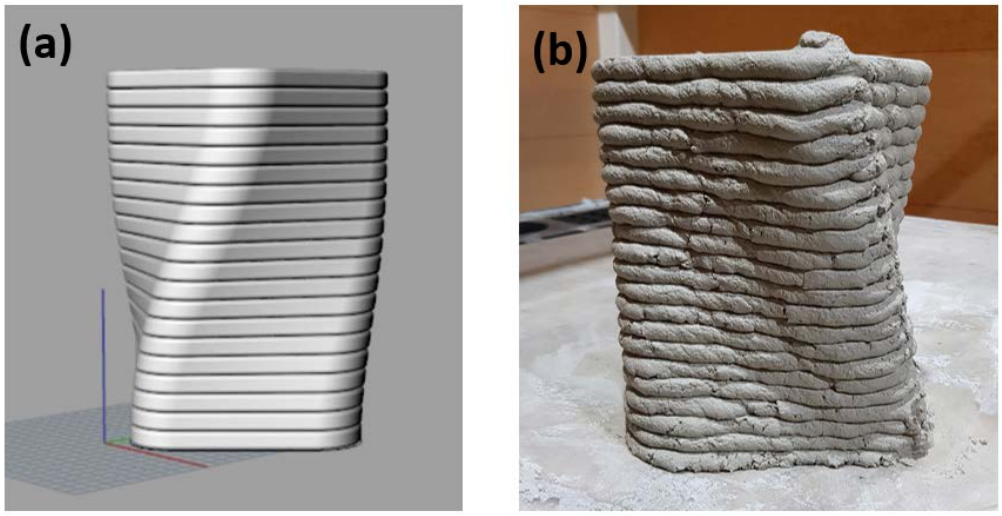

Fig. 10 3D twisted column generated by using the AAS mix containing 0.4% NC and 2% hydromagnesite seeds, showing: (a) 3D CAD model and (b) actual printed structure

3.4 Microstructural characterization

The feasibility of using the developed AAS mix in large-scale printing applications was further evaluated via the assessment of its microstructural properties Fig. 11 presents the XRD patterns of the AAS mix containing 0.4% NC and 0-2% hydromagnesite seeds after 14 days of curing. The main hydrate phase observed in both samples was C-(A)-S-H gel (i.e. 30-31° 2θ; PDF #00-033-0306), which was in line with the findings of previous studies [37, 38]. A comparison of the XRD patterns of both samples revealed the higher intensity of C-(A)-S-H in the seeded sample when compared with the unseeded sample. Along with C-(A)-S-H, a small amount of calcite ($CaCO_3$; PDF #01-071-3699) and hydrotalcite ($Mg_6Al_2CO_3(OH)_{16}\cdot 4(H_2O)$) were also observed. Furthermore, the microstructures of both samples, shown in Fig. 12, revealed the denser microstructure of the seeded sample in comparison to the unseeded sample. The wide-spread growth of C-(A)-S-H gel on the surfaces of the rosette-like hydromagnesite particles confirmed

the role of these seeds in providing additional nucleation sites for the increased precipitation of hydration products, which could lead to fast setting and improved early mechanical performance [36, 40].

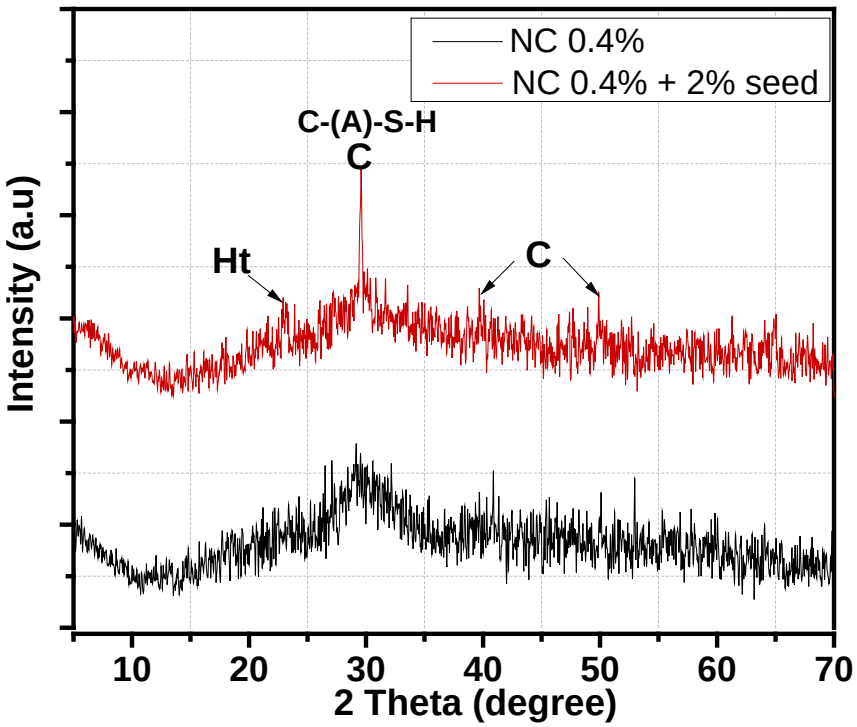

Fig. 11 XRD patterns of the AAS mix containing 0.4% NC and 0-2% hydromagnesite seeds after 14 days of curing (Ht: hydrotalcite and C: calcite)

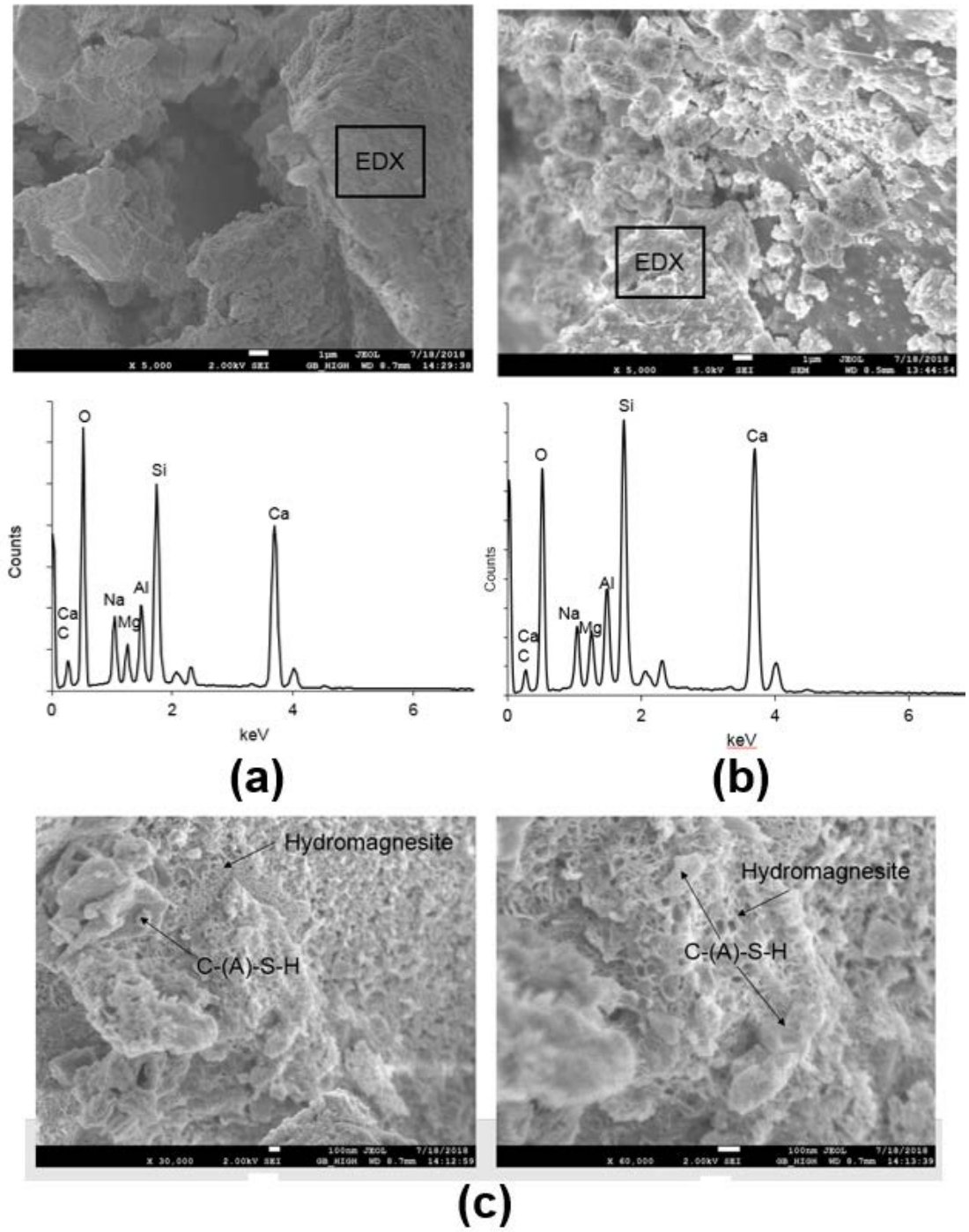

Fig. 12 SEM images and elemental composition of the AAS mix containing 0.4% NC and (a) 0% seeds and (b)-(c) 2% seeds

4. Conclusions

This paper aimed to improve the rheological properties of alkali-activated slag (AAS) binders for extrusion-based 3D printing. While slag was used as the main binder, different amounts of nanoclay (NC) were introduced to enable the development of extrudable and buildable (i.e. printable) mixes. Selected mixes were subjected to a range of rheological measurements to determine their yield stress, viscosity and thixotropy recovery required for 3D printing applications. The AAS mix by itself was found to exhibit a low yield stress due to the plasticizing and deflocculating effects of the silicate particles. Inclusion of 0.4% NC in these AAS mixes significantly improved the initial yield stress due to the flocculation effect. However, structural rebuilding rate remained unaffected even in the presence of NC and this was resolved via the addition of 2% hydromagnesite seeds, which can increase the rate of the hydration reaction and early strength development of AAS mixes, contributing to the buildability property necessary for large-scale concrete printing.

While this study has paved the way for the development of alternative binders with improved properties for 3D printing applications, further studies focusing on the optimization of the mix design in terms of the NC content and seed type could enable the end users to fully harvest the benefits of each additive in creating sustainable mixes with an enhanced performance.

Acknowledgements

The authors would like to acknowledge Sembcorp Architects & Engineers Pte. Ltd. and National Research Foundation (NRF) of Singapore for their funding and support of the work performed by Biranchi Panda and Ming Jen Tan. Shaoqin Ruan and Cise Unluer were supported by the Singapore MOE Academic Research Fund Tier 1 (RG 95/16).

References

1. Tay, Y.W.D., Panda, B., Paul, S.C., Noor Mohamed, N.A., Tan, M.J. and Leong, K.F., 2017. 3D printing trends in building and construction industry: a review. Virtual and Physical Prototyping, 12(3), pp.261-276.
2. Buswell, R.A., de Silva, W.L., Jones, S.Z. and Dirrenberger, J., 2018. 3D printing using concrete extrusion: A roadmap for research. Cement and Concrete Research, 112, pp.37-49.
3. De Schutter, G., Lesage, K., Mechtcherine, V., Nerella, V.N., Habert, G. and Agusti-Juan, I., 2018. Vision of 3D printing with concrete—technical, economic and environmental potentials. Cement and Concrete Research, 112, pp.25-36.
4. Ngo, T.D., Kashani, A., Imbalzano, G., Nguyen, K.T. and Hui, D., 2018. Additive manufacturing (3D printing): A review of materials, methods, applications and challenges. Composites Part B: Engineering, 143, pp.172-196.
5. Wangler, T., Roussel, N., Bos, F.P., Salet, T.A. and Flatt, R.J., 2019. Digital concrete: a review. Cement and Concrete Research, 123, p.105780.
6. Davtalab, O., Kazemian, A. and Khoshnevis, B., 2018. Perspectives on a BIM-integrated software platform for robotic construction through Contour Crafting. Automation in Construction, 89, pp.13-23.
7. Buswell, R.A., Thorpe, A., Soar, R.C. and Gibb, A.G., 2018. Design, data and process issues for mega-scale rapid manufacturing machines used for construction. Automation in Construction, 17(8), pp.923-929.
8. Agarwal, R., Chandrasekaran, S. and Sridhar, M., 2016. Imagining construction's digital future. McKinsey Productivity Sciences Center.
9. DebRoy, T., Zhang, W., Turner, J. and Babu, S.S., 2017. Building digital twins of 3D printing machines. Scripta Materialia, 135, pp.119-124.
10. Roussel, N., 2018. Rheological requirements for printable concretes. Cement and Concrete Research, 112, pp.76-85.
11. Lim, J.H., Panda, B. and Pham, Q.C., 2018. Improving flexural characteristics of 3D printed geopolymer composites with in-process steel cable reinforcement. Construction and Building Materials, 178, pp.32-41.

12. Asprone, D., Menna, C., Bos, F.P., Salet, T.A., Mata-Falcón, J. and Kaufmann, W., 2018. Rethinking reinforcement for digital fabrication with concrete. Cement and Concrete Research, 112, pp.111-121.
13. Ma, G., Li, Z., Wang, L., Wang, F. and Sanjayan, J., 2019. Mechanical anisotropy of aligned fiber reinforced composite for extrusion-based 3D printing. Construction and Building Materials, 202, pp.770-783.
14. Figueiredo, S.C., Rodríguez, C.R., Ahmed, Z.Y., Bos, D.H., Xu, Y., Salet, T.M., Çopuroğlu, O., Schlangen, E. and Bos, F.P., 2019. An approach to develop printable strain hardening cementitious composites. Materials & Design, 169, p.107651.
15. Le, T.T., Austin, S.A., Lim, S., Buswell, R.A., Gibb, A.G. and Thorpe, T., 2012. Mix design and fresh properties for high-performance printing concrete. Materials and structures, 45(8), pp.1221-1232.
16. Kazemian, A., Yuan, X., Cochran, E. and Khoshnevis, B., 2017. Cementitious materials for construction-scale 3D printing: Laboratory testing of fresh printing mixture. Construction and Building Materials, 145, pp.639-647.
17. Paul, S.C., Tay, Y.W.D., Panda, B. and Tan, M.J., 2018. Fresh and hardened properties of 3D printable cementitious materials for building and construction. Archives of civil and mechanical engineering, 18(1), pp.311-319.
18. Alghamdi, H., and Neithalath, N., 2019. Synthesis and characterization of 3D-printable geopolymeric foams for thermally efficient building envelope materials. Cement and Concrete Composites, 104, p.103377.
19. Panda, B., Paul, S.C., Hui, L.J., Tay, Y.W.D. and Tan, M.J., 2017. Additive manufacturing of geopolymer for sustainable built environment. Journal of cleaner production, 167, pp.281-288.
20. Bong, S.H., Nematollahi, B., Nazari, A., Xia, M. and Sanjayan, J.G., 2018, September. Fresh and hardened properties of 3D printable geopolymer cured in ambient temperature. In RILEM International Conference on Concrete and Digital Fabrication (pp. 3-11). Springer, Cham.
21. Chen, Y., Li, Z., Chaves Figueiredo, S., Çopuroğlu, O., Veer, F. and Schlangen, E., 2019. Limestone and Calcined Clay-Based Sustainable Cementitious Materials for 3D Concrete Printing: A Fundamental Study of Extrudability and Early-Age Strength Development. Applied Sciences, 9(9), p.1809.

22. Panda, B. and Tan, M.J., 2019. Rheological behavior of high-volume fly ash mixtures containing micro silica for digital construction application. Materials Letters, 237, pp.348-351.
23. Panda, B., Mohamed, N., Ahamed, N., Paul, S.C., Bhagath Singh, G.V.P., Tan, M.J. and Šavija, B., 2019. The Effect of Material Fresh Properties and Process Parameters on Buildability and Interlayer Adhesion of 3D Printed Concrete. Materials, 12(13), p.2149.
24. Dung, N.T. and Unluer, C., 2017. Influence of nucleation seeding on the performance of carbonated MgO formulations. Cement and Concrete Composites, 83, pp.1-9.
25. Dung, N.T. and Unluer, C., 2019. Performance of reactive MgO concrete under increased CO2 dissolution. Cement and Concrete Research, 118, pp.92-101.
26. Hubler, M.H., Thomas, J.J. and Jennings, H.M., 2011. Influence of nucleation seeding on the hydration kinetics and compressive strength of alkali activated slag paste. Cement and Concrete Research, 41(8), pp.842-846.
27. Panda, B. and Tan, M.J., 2018. Experimental study on mix proportion and fresh properties of fly ash based geopolymer for 3D concrete printing. Ceramics International, 44(9), pp.10258-10265.
28. Panda, B., Unluer, C. and Tan, M.J., 2018. Investigation of the rheology and strength of geopolymer mixtures for extrusion-based 3D printing. Cement and Concrete Composites, 94, pp.307-314.
29. Panda, B., Paul, S.C., Mohamed, N.A.N., Tay, Y.W.D. and Tan, M.J., 2018. Measurement of tensile bond strength of 3D printed geopolymer mortar. Measurement, 113, pp.108-116.
30. Standard Test Method for Measurement of Heat of Hydration of Hydraulic Cementitious Materials Using Isothermal Conduction Calorimetry. ASTM Committee C01, West Conshohocken, PA 19428-2959, United States (2015), p. 8
31. Kashani, A., Provis, J.L., Qiao, G.G. and van Deventer, J.S., 2014. The interrelationship between surface chemistry and rheology in alkali activated slag paste. Construction and Building Materials, 65, pp.583-591.
32. Panda, B., Ruan, S., Unluer, C. and Tan, M.J., 2019. Improving the 3D printability of high-volume fly ash mixtures via the use of nano attapulgite clay. Composites Part B: Engineering, 165, pp.75-83.

33. Dejaeghere, I., Sonebi, M. and De Schutter, G., 2019. Influence of nano-clay on rheology, fresh properties, heat of hydration and strength of cement-based mortars. Construction and Building Materials, 222, pp.73-85.
34. Panda, B., Lim, J.H. and Tan, M.J., 2019. Mechanical properties and deformation behaviour of early age concrete in the context of digital construction. Composites Part B: Engineering, 165, pp.563-571.
35. Reiter, L., Wangler, T., Roussel, N. and Flatt, R.J., 2018. The role of early age structural build-up in digital fabrication with concrete. Cement and Concrete Research, 112, pp.86-95.
36. Thomas, J.J., Jennings, H.M. and Chen, J.J., 2009. Influence of nucleation seeding on the hydration mechanisms of tricalcium silicate and cement. The Journal of Physical Chemistry C, 113(11), pp.4327-4334.
37. Wang, S.D. and Scrivener, K.L., 1995. Hydration products of alkali activated slag cement. Cement and Concrete Research, 25(3), pp.561-571.
38. Wang, S.D., Pu, X.C., Scrivener, K.L. and Pratt, P.L., 1995. Alkali-activated slag cement and concrete: a review of properties and problems. Advances in cement research, 7(27), pp.93-102.
39. Hasanzadeh, B. 2017. Testing and modeling of the thixotropic behavior of cementitious materials. PhD Thesis. University of Louisville.
40. Dung, N. T., Hooper, T. J. N., & Unluer, C. 2019. Accelerating the reaction kinetics and improving the performance of Na2CO3-activated GGBS mixes. Cement and Concrete Research, 126, 105927.